Image Deblurring via Enhanced Low-Rank Prior

Wenqi Ren, Xiaochun Cao, *Senior Member, IEEE*, Jinshan Pan, Xiaojie Guo, *Member, IEEE*, Wangmeng Zuo, *Senior Member, IEEE*, and Ming-Hsuan Yang, *Senior Member, IEEE*

***Abstract*— Low-rank matrix approximation has been successfully applied to numerous vision problems in recent years. In this paper, we propose a novel low-rank prior for blind image deblurring. Our key observation is that directly applying a simple low-rank model to a blurry input image significantly reduces the blur even without using any kernel information, while preserving important edge information. The same model can be used to reduce blur in the gradient map of a blurry input. Based on these properties, we introduce an enhanced prior for image deblurring by combining the low rank prior of similar patches from both the blurry image and its gradient map. We employ a weighted nuclear norm minimization method to further enhance the effectiveness of low-rank prior for image deblurring, by retaining the dominant edges and eliminating fine texture and slight edges in intermediate images, allowing for better kernel estimation. In addition, we evaluate the proposed enhanced low-rank prior for both the uniform and the non-uniform deblurring. Quantitative and qualitative experimental evaluations demonstrate that the proposed algorithm performs favorably against the state-of-the-art deblurring methods.**

***Index Terms*— Blind deblurring, low rank, weighted nuclear norm, non-uniform deblurring.**

I. Introduction

SINGLE image blind deblurring has recently attracted great attention in computer vision and numerous methods have been developed. The mathematical formulation of image blurring, under the assumption of uniform camera motion, can be modeled as,

$$b = l \otimes k + n, \tag{1}$$

where b, l and n are blurry observation, latent image and noise, respectively. In addition, k is the blur kernel and $\otimes$ denotes the convolution operator.

The goal of image deblurring is to recover the latent image l and the corresponding blur kernel k from one blurry input image b. This is a highly ill-posed problem, because many different pairs l and k can give rise to the same b. Thus, additional information is required to constrain the solutions. To make this problem well-posed, most existing methods usually use prior knowledge from the statistics of natural images and blur kernels, such as heavy-tailed gradient distributions [1]–[3], normalized sparsity prior [4], sparsity constraints [5] and L_0-regularized gradient [6], or a combination of both the intensity and gradient prior [7]. Most of the aforementioned methods are based on the image gradient which usually model the interactions between pixel pairs. It is difficult to model more complex structures of natural images only using adjacent image pixels, as natural images contain complex structures. To overcome this limitation, some patch prior-based methods have been proposed [8]–[13], which achieve state-of-the-art results in image denoising and non-blind image deblurring. Recently, the low-rank prior has been shown as a powerful patch prior, which is applied in image denoising and non-blind deblurring [12], [14]–[16] with significant improvements in performance.

In this paper, we propose a novel enhanced low rank prior for blind image deblurring (See Figure 1). We exploit the low rank properties of both intensity and gradient maps from image patches. To regularize the solution space of latent images, we formulate the problem as a weighted nuclear norm minimization task based on low rank properties. In addition, we extend our proposed low rank prior for non-uniform image deblurring. Experimental results on two benchmark datasets [3], [17] demonstrate that the proposed algorithm based on the enhanced low rank prior performs favorably against the state-of-the-art deblurring methods.

The contributions of this work are summarized as follows:

- We analyze the effect of low rank matrix approximation on blind image deblurring and propose a novel algorithm using low rank prior.
- We exploit the low rank properties of both intensity and gradient maps from an image to recover the intermediate image for kernel estimation. In the proposed low rank prior, we develop a method based on weighted nuclear

Manuscript received October 3, 2015; revised April 3, 2016; accepted May 9, 2016. Date of publication May 19, 2016; date of current version June 7, 2016. This work was supported in part by the National High-Tech Research and Development Program of China under Grant 2013CB329305, in part by the National Basic Research Program of China under Grant 2013CB329305, in part by the National Natural Science Foundation of China under Grant 61422213, Grant 61271093, and Grant 61402467, and in part by the Chinese Academy of Sciences through the Strategic Priority Research Program under Grant XDA06010701. The work of X. Guo was supported by the Chinese Academy of Sciences within the Institute Information Engineering through the Excellent Young Talent Programme. The work of M.-H. Yang was supported in part by the National Science Foundation (NSF) through the CAREER Program under Grant 1149783 and in part by NSF Grant 1152576 and in part by NSF within the Division of Information and Intelligent Systems through a Gift from Adobe. The associate editor coordinating the review of this manuscript and approving it for publication was Dr. Christopher Wyatt.

W. Ren and X. Cao are with the School of Computer Science and Technology, Tianjin University, Tianjin 300072, China (e-mail: rwq.renwenqi@gmail.com; caoxiaochun@iie.ac.cn).

J. Pan and M.-H. Yang are with the School of Engineering, University of California at Merced, Merced, CA 95343 USA (e-mail: sdluran@gmail.com; mhyang@ucmerced.edu).

X. Guo is with the State Key Laboratory of Information Security, Institute of Information Engineering, Chinese Academy of Sciences, Beijing 100093, China (e-mail: xj.max.guo@gmail.com).

W. Zuo is with the School of Computer Science and Technology, Harbin Institute of Technology, Harbin 150001, China (e-mail: cswmzuo@gmail.com).

Color versions of one or more of the figures in this paper are available online at http://ieeexplore.ieee.org.

Digital Object Identifier 10.1109/TIP.2016.2571062

(a) Blurry image (rank = 33) (b) Our result (rank=68)
(c) rank = 35 (d) rank = 25
(e) rank = 17 (f) rank = 9

Fig. 1. The proposed low rank prior favors clear intermediate results which helps kernel estimation. (a) A blurry input. (b) Final deblurred image by the proposed algorithm. (c) Intensity map of (a). (d) Result by applying the proposed low rank model (2) on (c) without kernel estimation. (e) Gradient map of (a). (f) Result by applying the proposed low rank model (2) on (e) without kernel estimation.

norm minimization to further enhance the effectiveness of low rank properties by eliminating fine texture details and small edges while preserving dominant edges.

- We extend the proposed algorithm based on low rank properties for non-uniform image deblurring caused by camera rotation.

II. Related Work and Problem Context

We discuss the related work on image priors for deblurring, low rank matrix approximation for vision problems, and some related non-uniform deblurring methods in this section.

A. Priors Based on Image Gradients

In order to estimate blur kernels from blurry images, statistical priors of gradient distributions have been modeled in various methods. Fergus *et al.* [1] exploit a mixture of Gaussians to fit the distribution of natural image gradients and the blur kernel estimation is obtained by variational Bayes inference. Shan *et al.* [2] introduce a method by concatenating two piece-wise continuous functions to fit the logarithmic gradient distribution of natural images and use that for image deblurring. In [18], Levin *et al.* model the latent images by a hyper-Laplacian prior and develop an efficient marginal approximation method to estimate blur kernels. As some image priors used in image deblurring favor blurry images rather than clear images [3], the normalized sparsity prior [4] and patch recurrence prior [19] have been proposed to overcome this problem. While these priors have been demonstrated for image deblurring, the priors used in these methods usually lead to highly non-convex models, which are computationally expensive. To reduce the computational load, the methods in [20] and [21] use Gaussian prior on the latent images and introduce an additional edge selection step for kernel estimation. However, the edge selection step is often based on heuristic filters and the assumption that there exist strong edges in the latent images may not always hold. To better reconstruct sharp edges for kernel estimation, exemplar based methods [17], [22], [23] have been proposed to exploit information contained both in a blurry input and example images. However, query in the external dataset is computationally expensive. In addition to generic priors, statistics for specific classes of objects (e.g., text and faces) have also been exploited [7], [22], [24] for deblurring.

B. Priors Based on Image Intensities

Sparse representations have recently been used to model image patches for deblurring [15]. In [25], Hu *et al.* learn an over-complete dictionary directly from a blurry image and use the sparsity constraints to iteratively recover the latent image. A sparse representation algorithm is proposed by Zhang *et al.* [26] to deblur and recognize face images jointly. Cai *et al.* [5] develop a deblurring method by enforcing sparsity constraints on both the sharp image and blur kernel using wavelets. In addition, Couzinie-Devy *et al.* [27] model the clear image patches and blurry ones with a linear mapping function, and learn a dictionary to restore the missing sharp details. A number of multi-scale dictionaries are used to describe and deblur text images by Cao *et al.* [28]. Although these dictionary-based methods may restore some high-textured regions, they do not carry substantially useful information for kernel estimation and often generate hallucinated high frequency contents, which complicate the subsequent kernel estimation steps [17].

C. Low Rank Matrix Approximation

In recent years, low rank matrix approximation (LRMA) methods have been developed and successfully applied to image modeling. Among which, the nuclear norm minimization (NNM) approach for LRMA has been successfully employed in numerous problems including robust principal component analysis [29], visual tracking [30], matrix denoising [31], matrix completion [32], [33] and low-level vision tasks [34]. The LRMA has also been applied to the non-blind image deblurring problem. A low rank based non-local spectral prior is exploited by Wang *et al.* [12] for non-blind image deblurring. Recently, Gu *et al.* [16] propose a weighted nuclear norm minimization (WNNM) algorithm that facilitates more flexible and robust results in image denoising. In contrast to the WNNM method [16] where a weighting scheme is designed specifically for denoising, we propose a novel algorithm to estimate weights for deblurring. In our method, the low rank prior is employed to generate the intermediate images by eliminating fine texture details and tiny edges while maintaining the dominant structures in blurry images, which play an important role for kernel estimation.

D. Some Related Non-Uniform Deblurring Methods

For non-uniform deblurring, Gupta *et al.* [35] propose a 3D approximation considering camera translation as well

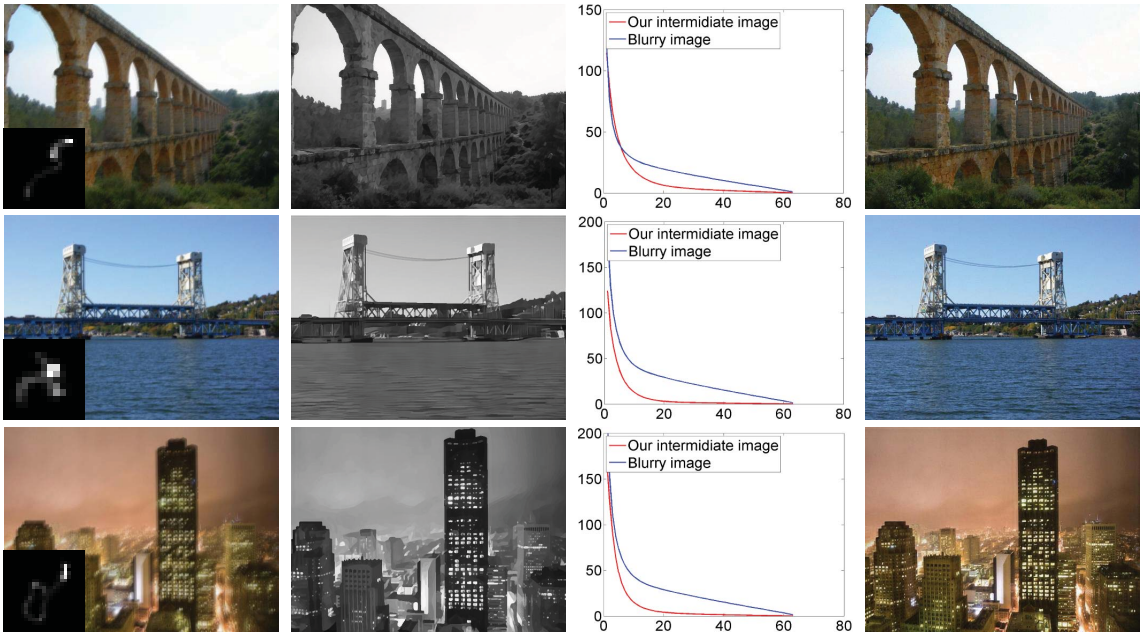

Fig. 2. Rank relationship between blurry and intermediate images. (a) Blurry inputs and kernels. (b) Intermediate images estimated by our method. (c) Distributions of average singular values of non-local similar patches from (a) and (b), respectively. (d) Final deblurred results. The rank of non-local matrices in the intermediate images are lower than that of the blurry images.

as in-plane rotation. Numerous approaches have since been developed with the state-of-the-art performance [36]–[38]. Hu and Yang [39] propose an efficient single image deblurring algorithm by restraining the possible camera poses in a low-dimensional subspace to reduce computational loads. It is shown in [40] that both the approximate 3D models [35], [36] generate good results instead of using the 6D transformation for camera motion. As these methods are computationally expensive, various methods based on locally uniform approximation [6], [41]–[43] have been developed.

III. LRMA for Image Deblurring

In this section, we first present the problem formulation of low rank matrix approximation and demonstrate the feasibility for blind image deblurring.

A. Weighted Nuclear Norm Minimization

Finding the desired low-rank approximation x from an observed matrix y can be solved by the nuclear norm minimization method, which has an analytical solution by penalizing the singular values of the observed matrix equally [29]. Nevertheless, singular values are of different importance and thus cannot be truncated with the same threshold. To this end, Gu *et al.* [16] propose a low rank matrix approximation algorithm based on weighted nuclear norm minimization,

$$\min_{x} \|y - x\|_F^2 + \|x\|_{w,*}, \tag{2}$$

where $\|x\|_{w,*}$ is the weighted nuclear norm defined by the sum of singular values and the corresponding non-negative weights. In this model, larger singular values are shrunk less and smaller singular values are shrunk more to preserve the major data components, thereby making this model flexible for dealing with numerous problems.

B. Feasibility of LRMA for Deblurring

One key observation in this work is that the LRMA model (2) can be used to deblur an image to certain degree without using any kernel information. Figure 1(d) shows that this model is able to deblur image pixels of Figure 1(c) (the intensity image of Figure 1(a)) by approximating the blurry input y with an low rank matrix x based on (2). As some slight blurry edges are removed, the rank of Figure 1(d) is lower than the one in Figure 1(c). Furthermore, the LRMA model can also be applied to gradient images. Figure 1(f) shows that the LRMA model is able to remove blurry pixels of Figure 1(e) (the gradient image of Figure 1(a)). In this work, we show that low rank properties of both intensity and gradient images can be exploited for effective deblurring (See Figure 1(b)).

The deblurring results obtained using low-rank matrix approximation can be explained with some examples. Figure 2 shows the patch based singular value maps of three blurry images (Figure 2(a)) and the corresponding intermediate images (Figure 2(b)), obtained by the proposed algorithm, are used for blur kernel estimation. For each local patch of 8×8 pixels, we collect 70 non-local similar patches and form a 64×70 matrix. The singular values of the matrix formed by these patches are computed by Singular Value Decomposition (SVD). Figure 2(c) shows that the average matrix rank of similar non-local patches in the intermediate unnatural images is lower than that of similar non-local patches in a blurry image. This is mainly because all the patches with rich textures and small edges are smoothed

such that only dominant edges are retained. As a result, the average rank of intermediate patches is inevitably lower than that of blurry similar patches. These intermediate images with dominant edges are critical for kernel estimation. The final deblurred images are shown in Figure 2(d). Therefore, it is feasible to exploit the low rank prior of intermediate images for kernel estimation.

IV. Proposed Algorithm

In this section, we present a LRMA-based model for blind image deblurring, and propose an efficient optimization algorithm to estimate blur kernels in Section V. We first consider the uniform case, and extend it to the non-uniform case in Section VI.

A. Problem Formulation

We formulate the deblurring problem within the maximum a posteriori (MAP) framework,

$$\begin{aligned}\{\hat{l},\hat{k}\} &= \arg\min_{l,k} p(l,k|b)\\ &= \arg\min_{l,k} p(b|l,k)p(k)p(l),\end{aligned} \tag{3}$$

where $p(k)$ and $p(l)$ are the priors of the blur kernel and latent image, respectively. We take negative log likelihood of (3) and have the proposed deblurring model as follows,

$$\{\hat{l},\hat{k}\} = \arg\min_{l,k} \ell(l\otimes k, b) + \gamma\phi(k) + \lambda\varphi(l), \tag{4}$$

and the details of each term in (4) are described below.

1) Data Fidelity Term: The first term in (4) is the data fidelity term, *i.e.*, the recovered image l should be consistent with the observation b. Its form depends on the assumed distribution of the noise model. The fidelity function $\ell(l\otimes k, b)$ usually penalizes the difference between $l\otimes k$ and b by using the ℓ_2-norm $\|l\otimes k - b\|_2^2$ as in [20] and [44]–[46]. However, it has been shown that such functions are sensitive to outliers than those based on the l_1-norm [21]. In this paper, we use the ℓ_1-norm [21] for the data fidelity term,

$$\ell(l\otimes k, b) = \|l\otimes k - b\|_1. \tag{5}$$

2) Kernel Prior: The second term is the constraint for the blur kernel, which is used to stabilize the solution of blur kernel k. In this paper, we use the l_2-norm on blur kernel k,

$$\phi(k) = \|k\|_2^2, \tag{6}$$

as it can be efficiently solved by the Fast Fourier Transform (FFT) [20], [21].

3) Image Prior: The last term in (4) is the image prior. As discussed in Section III, we exploit the low rank properties of non-local neighboring patches on both intensity and gradient maps for kernel estimation. By grouping the vectors formed by the non-local similar patches into a matrix, it is expected to have low rank properties and sparse singular values. The noisy and blurry pixels can be removed by shrinking the singular values in the LRMA process as illustrated in Figure 1(d) and (f). The non-local self-similarity based method has been applied in numerous vision tasks including denoising [16], super-resolution [47], non-blind deblurring [12], and image restoration [48]. We use the non-local self-similarity of both intensity and gradient patches based low rank prior for blind image deblurring by,

$$\varphi(l) = \sum_i \|l_i\|_* + \frac{\sigma}{\lambda}\sum_i \|\nabla l_i\|_*, \tag{7}$$

where $\nabla = (\nabla_h, \nabla_v)^\top$ denotes the image gradient operator. In addition, l_i and ∇l_i denote the matrices stacked by the non-local similar image and gradient patches, respectively. It has been shown that better approximation can be obtained by assigning different weights on different singular values in the LRMA process [16]. As shown in Figure 2(c), larger singular values (close to the left) should be shrunk less or not truncated since the corresponding patches contain important and representative information. We reformulate the prior in (7) with,

$$\varphi(l) = \sum_i \|l_i\|_{w,*} + \frac{\sigma}{\lambda}\sum_i \|\nabla l_i\|_{w,*}. \tag{8}$$

The weight vector w should be inversely proportional to the singular values of l or ∇l_i, *i.e.*, $\sigma(l_i)$ or $\sigma(\nabla l_i)$. We discuss more about the image prior based on intensities and gradients in Section V-A.

B. Objective Function

The proposed single image blind deblurring model is formulated as,

$$\begin{aligned}\{\hat{l},\hat{k}\} = \arg\min_{l,k} &\|l\otimes k - b\|_1 + \gamma\|k\|_2^2\\ &+ \lambda\sum_i \|l_i\|_{w,*} + \sigma\sum_i \|\nabla l_i\|_{w,*}.\end{aligned} \tag{9}$$

The elements in kernel k are subject to the constraints that $k_i \geq 0$ and $\sum_i k_i = 1$. As shown in (9), the intensity and gradient maps based low rank prior is exploited in the proposed model. On one hand, the low rank properties of intensity and gradient images effectively regularize the solution space of the possible latent intermediate images. On the other hand, well estimated blur kernels facilitate better solutions of latent images (which is discussed in the following sections).

V. Optimization

As it is difficult to solve the proposed model (9) directly, we use an efficient alternating minimization algorithm based on half-quadratic splitting. That is, we estimate intermediate latent images and blur kernels alternatively by assuming one of them is known. We discuss the subproblems for the variables of this objective function and present an efficient optimization algorithm to solve them.

A. Updating Latent Images

In this subproblem, we fix the blur kernel k and optimize the latent sharp image $\hat{l}$. The optimization problem (9) becomes,

$$\hat{l} = \arg\min_{l,k} \|l\otimes k - b\|_1 + \lambda\sum_i \|l_i\|_{w,*} + \sigma\sum_i \|\nabla l_i\|_{w,*}. \tag{10}$$

We propose an efficient algorithm to solve (10) based on the half-quadratic splitting technique [49]. By introducing new auxiliary variables d, p and g, where $g = (g_h, g_v)^\top$, we rewrite the energy function (10) as,

$$\hat{l} = \arg\min_{l} \|l \otimes k - b - d\|_2^2 + \beta\|l - p\|_2^2 + \tau\|\nabla l - g\|_2^2 + \eta\|d\|_1 + \lambda \sum_i \|p_i\|_{w,*} + \sigma \sum_i \|g_i\|_{w,*}, \quad (11)$$

where η, β and τ are positive parameters.

The above optimization problem (11) can be divided into four subproblems, in which we solve l, d, p, and g, separately. To solve l, the energy function (11) becomes,

$$\hat{l} = \min_{l} \|l \otimes k - b - d\|_2^2 + \beta\|l - p\|_2^2 + \tau\|\nabla l - g\|_2^2, \quad (12)$$

in which l can be solved efficiently using the FFT,

$$l = \mathcal{F}^{-1}\left(\frac{\overline{\mathcal{F}(k)}\mathcal{F}(b+d) + \beta\mathcal{F}(p) + \tau\mathcal{F}_g}{\overline{\mathcal{F}(k)}\mathcal{F}(k) + \beta + \tau\overline{\mathcal{F}(\nabla)}\mathcal{F}(\nabla)}\right), \quad (13)$$

where $\mathcal{F}_g = \overline{\mathcal{F}(\nabla_h)}\mathcal{F}(g_h) + \overline{\mathcal{F}(\nabla_v)}\mathcal{F}(g_v)$, $\mathcal{F}(\cdot)$ and $\mathcal{F}^{-1}(\cdot)$ denote the FFT and inverse FFT respectively, and $\overline{\mathcal{F}(\cdot)}$ is the complex conjugate operator. Given l, we compute d by minimizing,

$$\hat{d} = \arg\min_{d} \|l \otimes k - b - d\|_2^2 + \eta\|d\|_1. \quad (14)$$

The closed-form solution of (14) is obtained by one-dimensional shrinkage operator,

$$d = \text{sign}(l \otimes k - b)\max(\|l \otimes k - b\| - \eta, 0). \quad (15)$$

The subproblems with respect to p and g can each be estimated by solving,

$$\hat{p} = \arg\min_{p} \beta\|l - p\|_2^2 + \lambda \sum_i \|p_i\|_{w,*}, \quad (16)$$

and

$$\hat{g} = \arg\min_{g} \tau\|\nabla l - g\|_2^2 + \sigma \sum_i \|g_i\|_{w,*}, \quad (17)$$

where, similar to [16] we define the weight vector w as,

$$w_j = 2\sqrt{2m}/(\sigma_j(\cdot) + \epsilon). \quad (18)$$

In the above equation, $\sigma_j(\cdot)$ denotes $\sigma_j(l_i)$ and $\sigma_j(\nabla l_i)$ for (16) and (17), respectively. In (18), $\sigma_j(l_i)$ is the j^{th} singular value of l_i and $\sigma_j(\nabla l_i)$ is the j^{th} singular value of ∇l_i. In addition, m is the number of columns of matrix l_i or ∇l_i, *i.e.*, the selected number of similar patches, and ϵ is an infinitely small number.

In (18), the initial $\sigma_j(l_i)$ can be estimated by,

$$\hat{\sigma}_j^{(1)}(l_i) = \sqrt{\max(\sigma_j^2(b_i) - ms^2, 0)}, \quad (19)$$

where s is the kernel size. In subsequent iterations, similar to [16], $\sigma_j^{(t)}(l_i)$ is estimated by,

$$\hat{\sigma}_j^{(t)}(l_i) = \eta\sqrt{s^2 - (\sigma_j(b_i) - \sigma_j(l_i^{(t-1)}))}, \quad (20)$$

where t denotes the index of subsequent iterations. With the well-defined weight vector w, the singular values of $\hat{l}_i$ are shrunk by the generalized soft-thresholding operator $\mathcal{S}_w(\Sigma)_{ii}$,

$$\mathcal{S}_w(\Sigma)_{ii} = \max(\Sigma_{ii} - w_j, 0). \quad (21)$$

The definition of $\sigma_j(\nabla l_i)$ is analogous to $\sigma_j(l_i)$ and thus omitted. The proposed weight vector w and soft-thresholding operator $\mathcal{S}_w(\Sigma)_{ii}$ play important roles in eliminating fine texture details and tiny edges while maintaining the main structures in blurry images (See Section VII-A for details).

By applying the above procedures to each patch of intensity and gradient maps, the intermediate intensity image $\hat{l}$ and gradient map $\nabla\hat{l}$ can be reconstructed. Although these two energy functions (16) and (17) are non-convex, they can be solved efficiently by the WNNM method in [16]. Xie *et al.* [50] show that the WNNM problem can be equivalently transformed into a quadratic program with linear constraints. That is, the above subproblems can be readily solved by any convex optimization solver with a global optimal solution. Furthermore, when the weights are non-descending, the globally optimal solution can be obtained in closed-form.

B. Estimating Blur Kernels

In this subproblem, we fix the latent image l and optimize the blur kernel $\hat{k}$. The optimization problem (9) becomes,

$$\hat{k} = \arg\min_{k} \|k \otimes l - b\|_1 + \gamma\|k\|_2^2. \quad (22)$$

For efficiency and stability, we use the fast deblurring method [20] to estimate the blur kernel based on the gradient images and l_2-norm of data fidelity term,

$$\hat{k} = \arg\min_{k} \|k \otimes \nabla l - \nabla b\|_2^2 + \gamma\|k\|_2^2. \quad (23)$$

This is a least squares minimization problem with Tikhonov regularization, which leads to a closed-form solution for k,

$$\hat{k} = \mathcal{F}^{-1}\left(\frac{\overline{\mathcal{F}(\nabla l)}\mathcal{F}(\nabla b)}{\overline{\mathcal{F}(\nabla l)}\mathcal{F}(\nabla l) + \gamma}\right). \quad (24)$$

In practice, we use a multi-scale blind deconvolution approach for more reliable kernel estimation in a way similar to the state-of-the-art methods [1], [6], [44]. We construct the image pyramid $\{b_0, b_1, \ldots, b_n\}$ for an observed blurry image b_0 and estimate the kernel at coarsest level, and refine the kernel as we move up to the full resolution level b_0. We apply the state-of-the-art deblurring method [6] to estimate the blur kernels and latent images at the intermediate levels $\{b_1, \ldots, b_n\}$, and apply our algorithm to estimate the final blur kernel at the full resolution level b_0. The main steps of the proposed deblurring algorithm are presented in Algorithm 1.

The proposed blind image deblurring algorithm is based on the alternating minimization approach. The subproblems for solving l and k ((12) and (23)) have closed-form solutions, as in (13) and (24), respectively. The subproblems for solving p and g ((16) and (17)) converge to stationary points when using the method proposed by Gu *et al.* [16].

Algorithm 1 Deblurring by Enhanced Low Rank Prior

Input: Downsample the observed blurry image b to generate the image pyramid $\{b_0, b_1, \ldots, b_n\}$.
Estimate the blur kernels $\hat{k}_i$ and latent images $\hat{l}_i$ $(i = 1, 2, \ldots, n)$ in intermediate layers using [6] and output $\hat{k}_1$.
Upsample $\hat{k}_1$ to generate initial blur kernel k_0 for full resolution image b_0.
for $j = 1, 2, \ldots, 5$ **do**
    solve d by minimizing (15).
    $\beta \leftarrow 2\sigma$.
    repeat
        solve p by minimizing (16).
        $\tau \leftarrow 2\lambda$.
        repeat
            solve g by minimizing (17).
            solve l by minimizing (13).
            $\tau \leftarrow 3\tau$.
        until $\tau > \tau_{max}$.
        $\beta \leftarrow 3\beta$.
    until $\beta > \beta_{max}$
    solve blur kernel k by (24).
    $\lambda \leftarrow 0.9\lambda$, $\sigma \leftarrow 0.9\sigma$.
end for
With the final estimated kernel k, use the final deconvolution method [51] to generate the final output l.

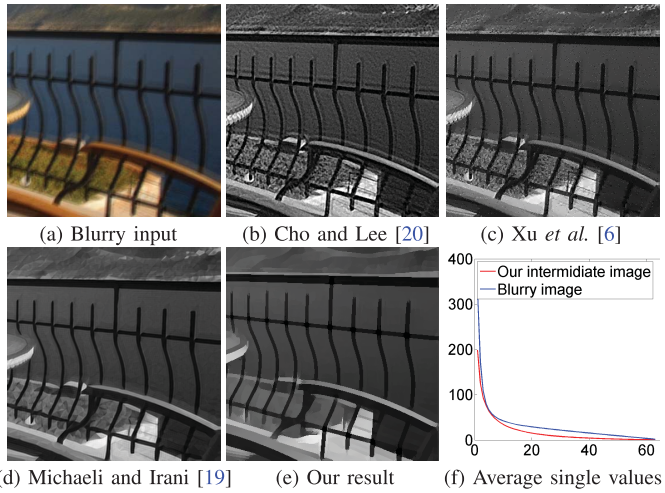

(a) Blurry input (b) Cho and Lee [20] (c) Xu *et al.* [6]
(d) Michaeli and Irani [19] (e) Our result (f) Average single values

Fig. 3. Intermediate images estimated by three state-of-the-art approaches [6], [19], [20] and the proposed algorithm. The intermediate images (b)-(d) have more blurry edges than (e) and the result in (c) by [6] contains some outliers. The average singular values of the blurry input and the intermediate image by our method are shown in (f). (best viewed on a high-resolution display).

C. Recovering Final Latent Image

As the main goal of this paper is to estimate blur kernels, we can use kinds of non-blind deconvolution methods to recover latent images once the blur kernel is determined. We note that although we can use (10) to estimate the final latent image, this method is less effective for the images with rich details (See Figure 3(e)). To recover a latent image with fine details, we use the non-blind deconvolution method [51] in this paper.

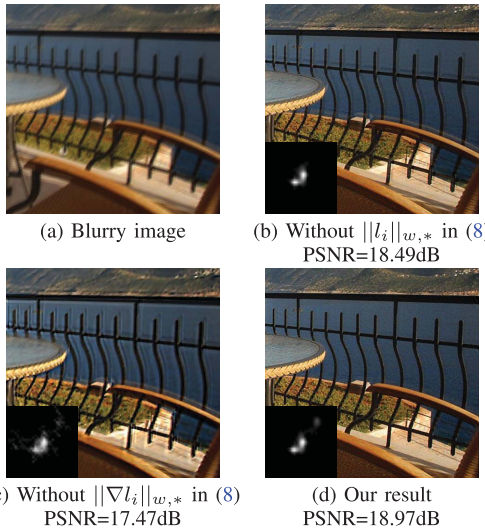

(a) Blurry image (b) Without $||l_i||_{w,*}$ in (8) PSNR=18.49dB
(c) Without $||\nabla l_i||_{w,*}$ in (8) PSNR=17.47dB (d) Our result PSNR=18.97dB

Fig. 4. Effectiveness of the proposed prior. (a) Blurry input. (b) Deblurred result based on the gradient map without the intensity map $||l_i||_{w,*}$ in (8). (c) Deblurred result based only on the intensity map without the gradient map $||\nabla l_i||_{w,*}$ in (8). (d) Deblurred result using the proposed algorithm.

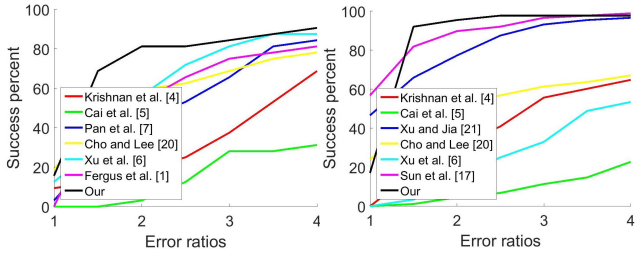

(a) (b)

Fig. 5. Quantitative evaluations on two benchmark datasets [3], [17]. (a) Results on [3]. (b) Results on [17].

VI. LRMA for Non-Uniform Deblurring

Camera shake including rotation and translation usually leads to spatially variant blur effect on images. This process is usually modeled as [6], [35],

$$\mathbf{b} = \sum_m k_m \mathbf{H}_m \mathbf{l} + \mathbf{n}, \tag{25}$$

where $\mathbf{b}$, $\mathbf{l}$ and $\mathbf{n}$ are the corresponding vector forms of b, l and n, respectively; m indexes camera pose samples and $\mathbf{H}_m$ is a transformation matrix which corresponds to either camera rotation or translation for pose m; and k_m denotes the time that the camera stays at pose m and serves as a weight in this function.

We note that the proposed low rank priors can be directly applied to non-uniform deblurring problems within the MAP framework. Based on the MAP formulation (3), the non-uniform deblurring model can be written as,

$$\{\hat{\mathbf{l}}, \hat{\mathbf{k}}\} = \arg\min_{\mathbf{l},\mathbf{k}} \| \sum_m k_m \mathbf{H}_m \mathbf{l} - \mathbf{b}\|_1 + \gamma\, \phi(\mathbf{k}) + \lambda \varphi(\mathbf{l}), \tag{26}$$

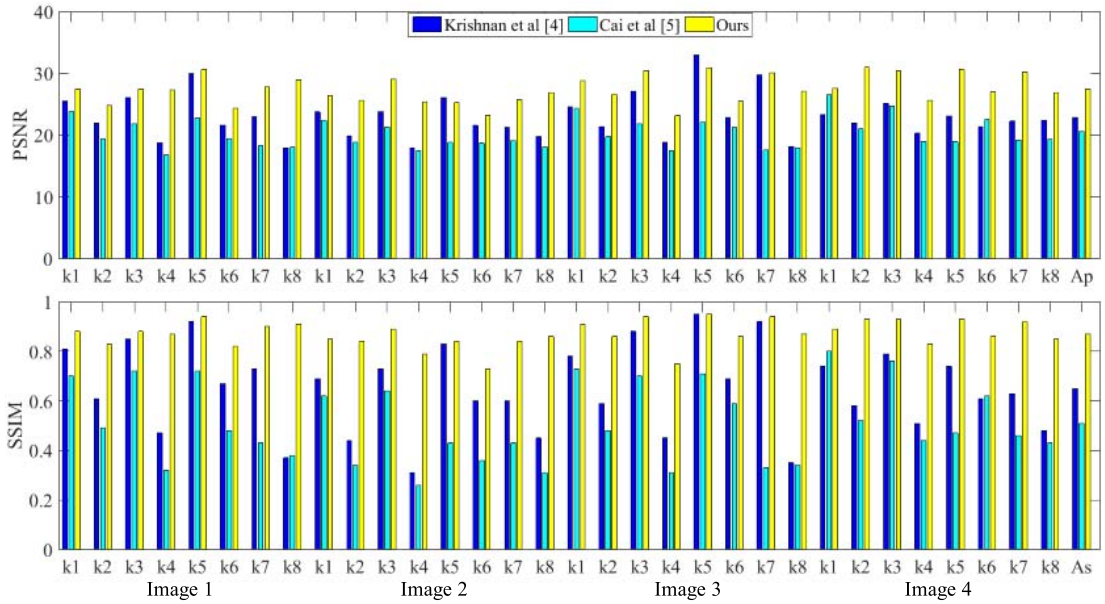

Fig. 6. Quantitative evaluation in terms of PSNR and SSIM on the dataset [3]. The numbers below the horizontal axis denote the kernel and image index and the Ap and As on the rightmost columns denote the average PSNR and SSIM of all these images. Overall, the proposed algorithm performs favorably against the representative state-of-the-art methods with priors based on image gradients and sparse representations.

Fig. 7. Evaluation against representative methods with priors based on image gradients [4] and sparse representation [5]. (a) Ground blur kernels and blurred images. (b) Krishnan *et al.* [4]. (c) Cai *et al.* [5]. (d) Our results without $\|l_i\|_{w,*}$. (e) Our results without $\|\nabla l_i\|_{w,*}$. (f) Our results.

where $\phi(\mathbf{k})$ and $\varphi(\mathbf{l})$ are defined in (6) and (8), and $\mathbf{k} = \{k_m\}$. The solution for (26) can be obtained by alternatively solving,

$$\hat{\mathbf{l}} = \arg\min_{\mathbf{l}} \| \sum_m k_m \mathbf{H}_m \mathbf{l} - \boldsymbol{b} \|_1 + \lambda \varphi(\mathbf{l}), \tag{27}$$

and

$$\hat{\mathbf{k}} = \arg\min_{\mathbf{k}} \| \sum_m k_m \mathbf{H}_m \mathbf{l} - \mathbf{b} \|_1 + \gamma \phi(\mathbf{k}). \tag{28}$$

For (27), we use the locally-uniform approximation [43] together with the optimization method described in Section V-A to solve this model. Similar to (10), the solution of (27) can be approximated by the solution of,

$$\begin{aligned} \hat{\mathbf{l}} = \arg\min_{\mathbf{l}} \| \sum_m k_m \mathbf{H}_m \boldsymbol{l} - \mathbf{b} - \mathbf{d} \|_2^2 + \beta \| \mathbf{l} - \mathbf{p} \|_2^2 \\ + \tau \| \nabla \mathbf{l} - \mathbf{g} \|_2^2 + \eta \| \mathbf{d} \|_1 + \lambda \sum_i \| \mathbf{p}_i \|_{w,*} \\ + \sigma \sum_i \| \nabla \mathbf{g}_i \|_{w,*}, \end{aligned} \tag{29}$$

where $\mathbf{d}$, $\mathbf{p}$ and $\mathbf{g}$ are the corresponding vector forms of d, p and g, respectively.

The optimization problem (29) can be divided into five subproblems, in which we solve for $\boldsymbol{l}$, k_m, $\boldsymbol{d}$, $\boldsymbol{p}$ and $\boldsymbol{g}$, separately. We use (15), (16) and (17) to update $\boldsymbol{d}$, $\boldsymbol{p}$ and $\boldsymbol{g}$. The method in [43] is used to update $\boldsymbol{l}$. As to the kernel estimation model (28), we use the same optimization method in [6] to update blur kernel k_m.

VII. Experimental Results

We carry out experiments on both synthesized and real images to evaluate the proposed algorithm against the state-of-the-art deblurring methods. Several metrics including peak-signal-to-noise ratios (PSNR), structural similarity (SSIM), kernel similarity (KSIM) and cumulative distributions of error ratio are used for performance evaluation on kernel estimations and deblurred images. In all the experiments, we use the following fixed parameters: $\gamma = 5$, $\lambda = \sigma = 0.05$, $\eta = 1$, $\beta_{max} = 2$ and $\tau_{max} = 8$. We use 8×8

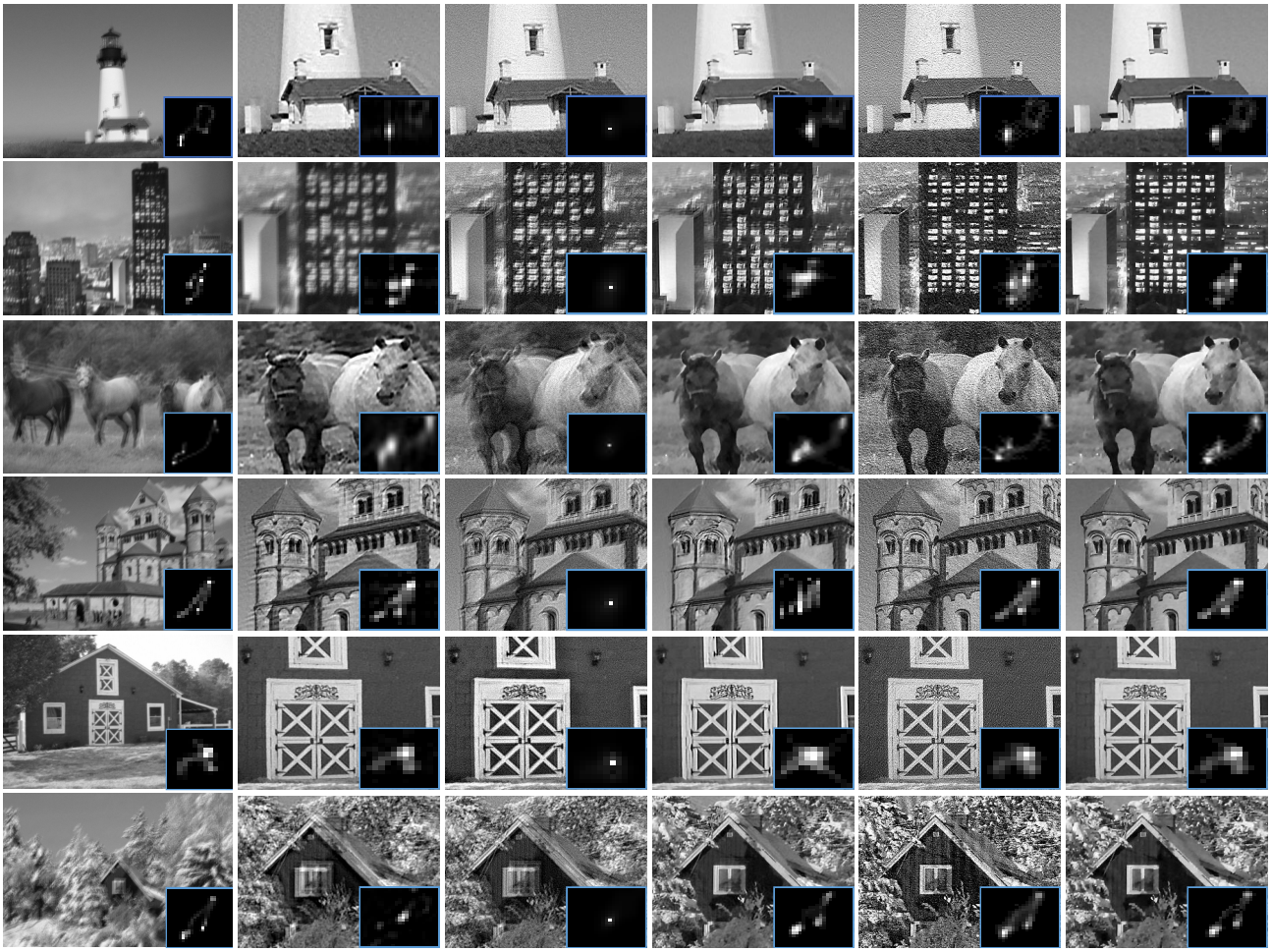

(a) (b) (c) (d) (e) (f)

Fig. 8. Deblurring results on six image regions from the dataset by Sun *et al.* [17]. Note that the kernels estimated by the proposed algorithm are close to the ground truth data while the state-of-the-art methods tend to introduce noise in the estimated kernels. Although the kernels are estimated well by [7], the final deblurred images contain more noise than other methods. (images best viewed on a high-resolution display). (a) Blurry images. (b) Krishnan *et al.* [4]. (c) Cai *et al.* [5]. (d) Zhong *et al.* [44]. (e) Pan *et al.* [7]. (f) Our results.

TABLE I

IMAGE DEBLURRING RESULTS OF AVERAGE METRICS (PSNR, SSIM AND KS) USING DIFFERENT METHODS CORRESPONDING TO FIGURE 8

Average Metrics	PSNR	SSIM	KSIM
Krishnan *et al.* [4]	20.43	0.53	0.43
Cai *et al.* [5]	17.08	0.21	0.19
Zhong *et al.* [44]	18.33	0.49	0.28
Pan *et al.* [7]	14.51	0.16	0.54
Ours	**22.56**	**0.68**	**0.60**

patches in blurry images with overlap of 1 pixel between adjacent patches. For each patch, we determine similar ones using the block matching algorithm [16] in a neighborhood of 30×30 pixels.

A. Effectiveness of Low Rank Prior

We first illustrate the effectiveness of low rank prior using an example with intermediate images generated by three state-of-the-art deblurring methods [6], [19], [20] and the proposed algorithm. As shown in Figure 3(b)-(d), the intermediate results by [19], [20] and [6] contain more blurry edges and notable outliers while the intermediate image generated by the proposed algorithm (Figure 3(e)) generates sharp edges which effectively help the kernel estimation process. In Figure 3(e), the textured patches and the patches including small edges are all smoothed, e.g., grass lawn, and thus the average rank of these intermediate patches is lower than those from the blurry similar patches. Figure 3(f) shows the average singular values of the matrices formed by the blurry and intermediate image patches, respectively.

In order to better understand how the priors of intensity and gradient affect our method, we show experimental results with different setups in Figure 4. Figure 4(b) and (c) show that clear images cannot be obtained by using the low rank properties of only gradient or intensity map, while the deblurred image obtained by low rank properties of both intensity and gradient maps have high visual quality and PSNR. These results indicate that the proposed prior $\varphi(l)$ in (8) plays a critical role in image deblurring.

B. Synthetic Images

In this section, we quantitatively evaluate the state-of-the-art deblurring methods as well as the proposed algorithm on two datasets with synthetically blurred images [3], [17].

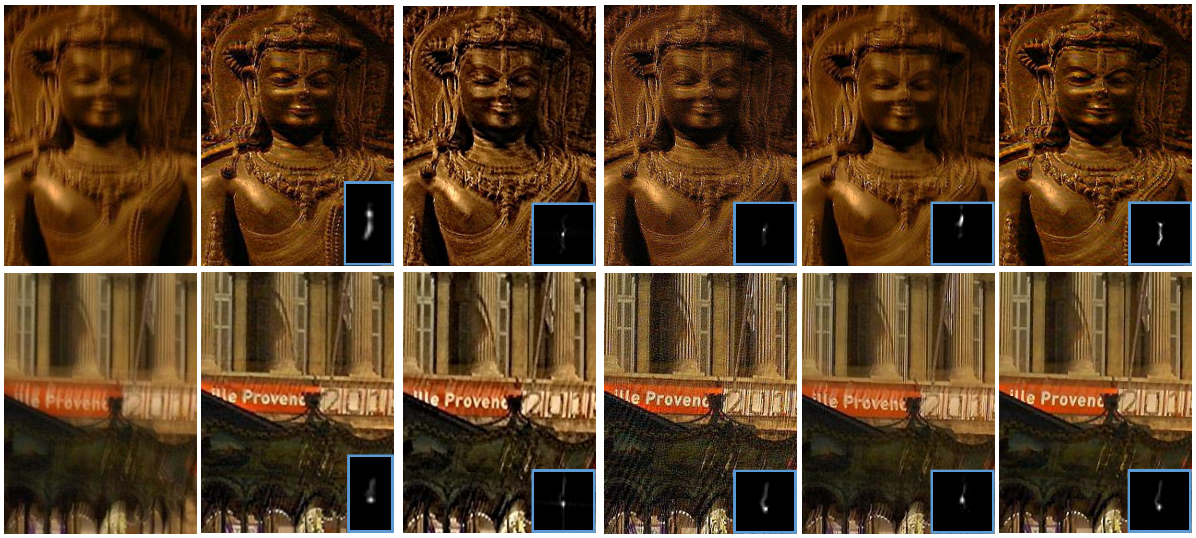

(a) (b) (c) (d) (e) (f)

Fig. 9. Visual comparison of state-of-the-art methods. These two blurry images in (a) are from [21]. (a) Blurry images. (b) Xu and Jia [21]. (c) Krishnan *et al.* [4]. (d) Xu *et al.* [6]. (e) Zhong *et al.* [44]. (f) Our results.

(a) (b) (c) (d) (e) (f)

Fig. 10. Visual comparison of state-of-the-art methods. The blurry image in (a) is from [44]. (a) Blurry images. (b) Krishnan *et al.* [4]. (c) Xu *et al.* [6]. (d) Zhong *et al.* [44]. (e) Pan *et al.* [7]. (f) Our results.

1) Dataset by Levin et al. [3]: We use the set of 32 images generated from 4 images and 8 different kernels, and compare the proposed algorithm with the state-of-the-art deblurring methods [1], [4]–[7], [20].

Figure 5(a) shows that the proposed algorithm based on low rank prior performs well against the state-of-the-art methods on this benchmark dataset in terms of cumulative error ratio. We compare two representative methods that utilize priors based on image gradients and sparse representation [4], [5], and report the PSNR and SSIM performance on each image in Figure 6. Two images from this dataset and the deblurred results are shown in Figure 7. Note that the kernels estimated by [4] contain some noise in certain directions, and the kernels computed by [5] contain a few bright regions along the camera shake trajectory.

To further understand the low rank priors of intensity and gradient, we show the results using the proposed algorithm without $\|l_i\|_{w,*}$ or $\|\nabla l_i\|_{w,*}$ in Figure 7(d) and (e), respectively. As shown in Figure 7(d), the estimated kernels are incorrect and the recovered images still contain blurry edges when without the intensity prior $\|l_i\|_{w,*}$. In Figure 7(e), the estimated kernels are similar to the ground truth without using $\|\nabla l_i\|_{w,*}$, but can still be improved with the gradient prior as in Figure 7(f). In contrast, the kernels estimated by the proposed algorithm are most similar to the ground truth, and the recovered latent images contain fewer artifacts.

2) Dataset by Sun et al. [17]: We carry out experiments on blurry and noisy images using the dataset by Sun *et al.* [17]. This dataset includes 640 images generated by 80 high resolution natural images from diverse scenes and 8 kernels. In addition, 1% Gaussian noise is added to each blurry image.

Figure 8 shows a few estimated kernels and deblurred images obtained by the proposed algorithm and the state-of-the-art methods [4], [5], [22], [44]. Note that the kernels estimated by the proposed algorithm are close to the ground truth whereas the results by existing methods contain a significant amount of noise or are close to delta functions [4], [5]. The deblurred images by [44] contain ringing artifacts, and the estimated kernels are noisy as shown in Figure 8(d). The deblurring method by [7] performs well on kernel estimation, but the final deblurred images contain some artifacts.

For the images shown in Figure 8, we present the PSNR, SSIM and KSIM values, averaged over all 8 kernels, of each deblurred result by the evaluated methods in Table I.

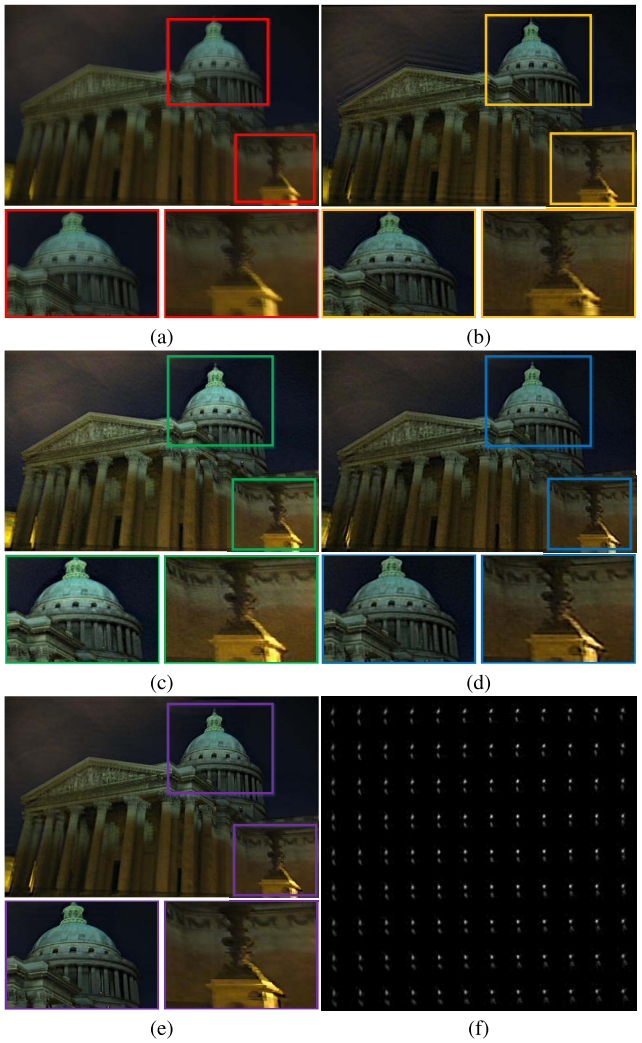

Fig. 11. Deblurring results of the *Pantheon* image with state-of-the-art non-uniform deblurring methods (best viewed on high-resolution display). (a) Blurry image. (b) Whyte *et al.* [36]. (c) Hirsch *et al.* [43]. (d) Xu *et al.* [6]. (e) Our result. (f) Our estimated kernels.

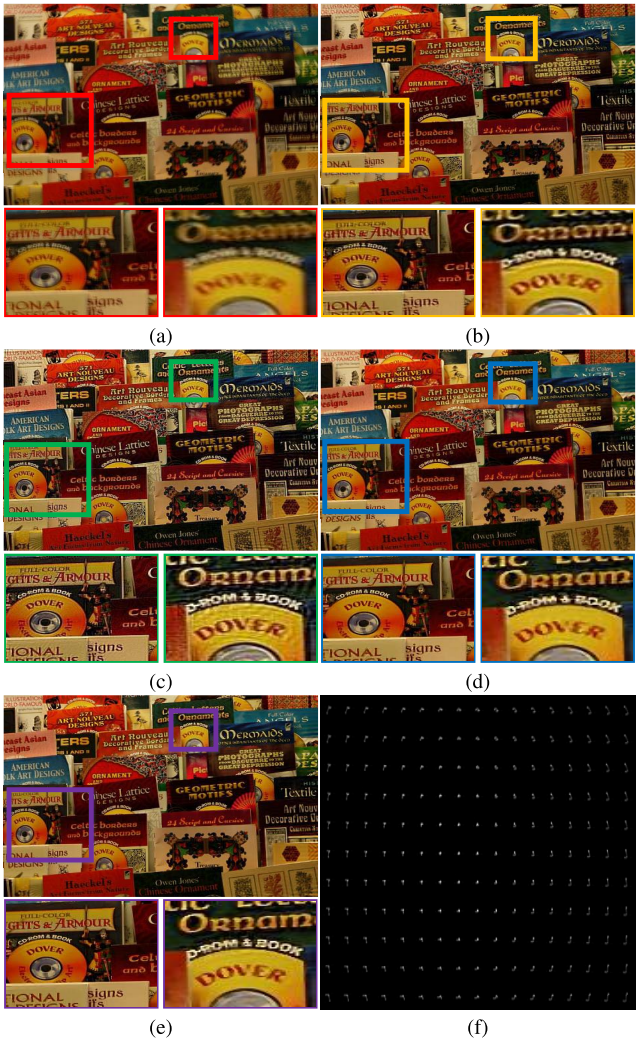

Fig. 12. Deblurring results of the *Book* image with state-of-the-art non-uniform deblurring methods (best viewed on high-resolution display). (a) Blurry image. (b) Gupta *et al.* [35]. (c) Hu and Yang [39]. (d) Xu *et al.* [6]. (e) Our result. (f) Our estimated kernels.

Overall, the proposed algorithm performs well in terms of the evaluation metrics. The method by Pan *et al.* [7] performs well in terms of kernel similarity. However, the final deblurred images generated by [7] consistently contain some noise. In addition, the PSNR as well as SSIM values are lower than those of other methods. Figure 5(b) shows that the proposed algorithm performs well on this dataset against the state-of-the-art deblurring methods [4]–[6], [17], [20], [21] in terms of cumulative error ratio, especially when the value is lower than 2 (which is closer to real-world scenarios).

C. Real Images

We use the real images [21], [44] to compare the proposed algorithm against the state-of-the-art blind single image deblurring methods [4], [6], [7], [20], [21], [44]. Since the ground truth images and kernels are unknown in these cases, we analyze the deblurring results qualitatively.

Figure 9 shows the deblurring results on two images from [21]. The deblurred images generated by the proposed algorithm are sharper and clearer whereas those recovered by other methods contain ringing artifacts. In addition, the kernels estimated by [4] and [44] in the second row of Figure 9 contain some image noise. Figure 10 shows the deblurring results on a real image, in which the estimated kernel is of 55×55 pixels [44]. The kernel estimated by the proposed algorithm contains less noise or outliers. Note that in Figure 10 and the first row of Figure 9, the deblurred texts by the proposed algorithm are clearer and sharper than those of other methods.

D. Non-Uniform Deblurring

In this section, we show that the proposed low rank priors can also be used for non-uniform deblurring problems. We compare the proposed non-uniform deblurring algorithm with the state-of-the-art non-uniform methods [6], [35], [36], [39], [43].

For the *Pantheon* image in Figure 11, the result from [36] contains ringing effects along the roof. Compared to [6] and [43], the proposed algorithm generates sharper results, as shown in the zoomed-in regions of Figure 11.

For the *Book* image in Figure 12, the results by [35] and [39] contain blurry edges around the texts

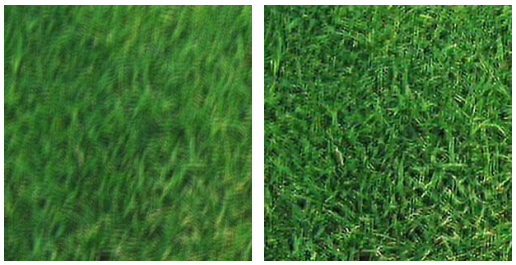

(a) (b)

Fig. 13. A failure example. The proposed algorithm fails to recover the clear image when the blurred image contains rich textures. (a) Blurry image. (b) Our result.

(See Figure 12(b) and (c)). Compared to [6], the proposed generates a comparable result with much clearer characters.

E. Failure Cases

As mentioned in Section III, the proposed method is able to shrink small singular values which usually correspond to textures in an image. Thus, the proposed method will fail if a blurred image contains rich textures, because most of textures will be removed and few sharp edges are retained for kernel estimation. Figure 13 shows an example and the deblurred result of the proposed methods. As the blurry image contains rich textures (*e.g.*, grass), the proposed method fails to generate clear results and the deblurred result contains obvious ringing artifacts.

VIII. Conclusions

In this paper, we present a novel enhanced low rank prior for blind image deblurring. The low rank properties of both intensity and gradient maps from image patches are exploited in the proposed algorithm. We present a weighted nuclear norm minimization approach based low rank properties to effectively recover latent images. Experimental results on benchmark datasets show that the proposed algorithm performs favorably against the state-of-the-art deblurring methods.

References

[1] R. Fergus, B. Singh, A. Hertzmann, S. T. Roweis, and W. T. Freeman, "Removing camera shake from a single photograph," *ACM Trans. Graph.*, vol. 25, no. 3, pp. 787–794, 2006.

[2] Q. Shan, J. Jia, and A. Agarwala, "High-quality motion deblurring from a single image," *ACM Trans. Graph.*, vol. 27, no. 3, p. 73, 2008.

[3] A. Levin, Y. Weiss, F. Durand, and W. T. Freeman, "Understanding and evaluating blind deconvolution algorithms," in *Proc. IEEE Conf. Comput. Vis. Pattern Recognit.*, Jun. 2009, pp. 1964–1971.

[4] D. Krishnan, T. Tay, and R. Fergus, "Blind deconvolution using a normalized sparsity measure," in *Proc. IEEE Conf. Comput. Vis. Pattern Recognit.*, Jun. 2011, pp. 233–240.

[5] J.-F. Cai, H. Ji, C. Liu, and Z. Shen, "Framelet-based blind motion deblurring from a single image," *IEEE Trans. Image Process.*, vol. 21, no. 2, pp. 562–572, Feb. 2012.

[6] L. Xu, S. Zheng, and J. Jia, "Unnatural L_0 sparse representation for natural image deblurring," in *Proc. IEEE Conf. Comput. Vis. Pattern Recognit.*, Jun. 2013, pp. 1107–1114.

[7] J. Pan, Z. Hu, Z. Su, and M.-H. Yang, "Deblurring text images via L_0-regularized intensity and gradient prior," in *Proc. IEEE Conf. Comput. Vis. Pattern Recognit.*, Jun. 2014, pp. 2901–2908.

[8] D. Zoran and Y. Weiss, "From learning models of natural image patches to whole image restoration," in *Proc. IEEE Int. Conf. Comput. Vis.*, Nov. 2011, pp. 479–486.

[9] S. Roth and M. J. Black, "Fields of experts," *Int. J. Comput. Vis.*, vol. 82, no. 2, pp. 205–229, Apr. 2009.

[10] U. Schmidt, Q. Gao, and S. Roth, "A generative perspective on MRFs in low-level vision," in *Proc. IEEE Conf. Comput. Vis. Pattern Recognit.*, Jun. 2010, pp. 1751–1758.

[11] J. Mairal, F. Bach, J. Ponce, G. Sapiro, and A. Zisserman, "Non-local sparse models for image restoration," in *Proc. IEEE 12th Int. Conf. Comput. Vis.*, Sep./Oct. 2009, pp. 2272–2279.

[12] S. Wang, L. Zhang, and Y. Liang, "Nonlocal spectral prior model for low-level vision," in *Proc. 11th Asian Conf. Comput. Vis.*, 2013, pp. 231–244.

[13] W. Dong, L. Zhang, G. Shi, and X. Wu, "Image deblurring and super-resolution by adaptive sparse domain selection and adaptive regularization," *IEEE Trans. Image Process.*, vol. 20, no. 7, pp. 1838–1857, Jul. 2011.

[14] W. Dong, G. Shi, and X. Li, "Nonlocal image restoration with bilateral variance estimation: A low-rank approach," *IEEE Trans. Image Process.*, vol. 22, no. 2, pp. 700–711, Feb. 2013.

[15] W. Dong, L. Zhang, G. Shi, and X. Li, "Nonlocally centralized sparse representation for image restoration," *IEEE Trans. Image Process.*, vol. 22, no. 4, pp. 1620–1630, Apr. 2013.

[16] S. Gu, L. Zhang, W. Zuo, and X. Feng, "Weighted nuclear norm minimization with application to image denoising," in *Proc. IEEE Conf. Comput. Vis. Pattern Recognit.*, Jun. 2014, pp. 2862–2869.

[17] L. Sun, S. Cho, J. Wang, and J. Hays, "Edge-based blur kernel estimation using patch priors," in *Proc. IEEE Int. Conf. Comput. Photogr.*, Apr. 2013, pp. 1–8.

[18] A. Levin, Y. Weiss, F. Durand, and W. T. Freeman, "Efficient marginal likelihood optimization in blind deconvolution," in *Proc. IEEE Conf. Comput. Vis. Pattern Recognit.*, Jun. 2011, pp. 2657–2664.

[19] T. Michaeli and M. Irani, "Blind deblurring using internal patch recurrence," in *Proc. 13th Eur. Conf. Comput. Vis.*, 2014, pp. 783–798.

[20] S. Cho and S. Lee, "Fast motion deblurring," *ACM Trans. Graph.*, vol. 28, no. 5, p. 145, 2009.

[21] L. Xu and J. Jia, "Two-phase kernel estimation for robust motion deblurring," in *Proc. 11th Eur. Conf. Comput. Vis.*, 2010, pp. 157–170.

[22] J. Pan, Z. Hu, Z. Su, and M.-H. Yang, "Deblurring face images with exemplars," in *Proc. Eur. Conf. Comput. Vis.*, 2014, pp. 47–62.

[23] Y. Hacohen, E. Shechtman, and D. Lischinski, "Deblurring by example using dense correspondence," in *Proc. IEEE Int. Conf. Comput. Vis.*, Dec. 2013, pp. 2384–2391.

[24] H. Cho, J. Wang, and S. Lee, "Text image deblurring using text-specific properties," in *Proc. 12th Eur. Conf. Comput. Vis.*, 2012, pp. 524–537.

[25] Z. Hu, J.-B. Huang, and M.-H. Yang, "Single image deblurring with adaptive dictionary learning," in *Proc. IEEE Int. Conf. Image Process.*, Sep. 2010, pp. 1169–1172.

[26] H. Zhang, J. Yang, Y. Zhang, N. M. Nasrabadi, and T. S. Huang, "Close the loop: Joint blind image restoration and recognition with sparse representation prior," in *Proc. IEEE Int. Conf. Comput. Vis.*, Nov. 2011, pp. 770–777.

[27] F. Couzinie-Devy, J. Mairal, F. Bach, and J. Ponce. (2011). "Dictionary learning for deblurring and digital zoom." [Online]. Available: http://arxiv.org/abs/1110.0957

[28] X. Cao, W. Ren, W. Zuo, X. Guo, and H. Foroosh, "Scene text deblurring using text-specific multiscale dictionaries," *IEEE Trans. Image Process.*, vol. 24, no. 4, pp. 1302–1314, Apr. 2015.

[29] E. J. Candès, X. Li, Y. Ma, and J. Wright, "Robust principal component analysis?" *J. ACM*, vol. 58, no. 3, p. 11, May 2011.

[30] T. Zhang, B. Ghanem, S. Liu, and N. Ahuja, "Low-rank sparse learning for robust visual tracking," in *Proc. 12th Eur. Conf. Comput. Vis.*, 2010, pp. 470–484.

[31] D. L. Donoho, M. Gavish, and A. Montanari, "The phase transition of matrix recovery from Gaussian measurements matches the minimax MSE of matrix denoising," *Proc. Nat. Acad. Sci.*, vol. 110, no. 21, pp. 8405–8410, 2013.

[32] J.-F. Cai, E. J. Candès, and Z. Shen, "A singular value thresholding algorithm for matrix completion," *SIAM J. Optim.*, vol. 20, no. 4, pp. 1956–1982, 2010.

[33] D. Zhang, Y. Hu, J. Ye, X. Li, and X. He, "Matrix completion by truncated nuclear norm regularization," in *Proc. IEEE Conf. Comput. Vis. Pattern Recognit.*, Jun. 2012, pp. 2192–2199.

[34] T.-H. Oh, H. Kim, Y.-W. Tai, J.-C. Bazin, and I. S. Kweon, "Partial sum minimization of singular values in RPCA for low-level vision," in *Proc. IEEE Int. Conf. Comput. Vis.*, Dec. 2013, pp. 145–152.

[35] A. Gupta, N. Joshi, C. L. Zitnick, M. Cohen, and B. Curless, "Single image deblurring using motion density functions," in *Proc. 11th Eur. Conf. Comput. Vis.*, 2010, pp. 171–184.

[36] O. Whyte, J. Sivic, A. Zisserman, and J. Ponce, "Non-uniform deblurring for shaken images," *Int. J. Comput. Vis.*, vol. 98, no. 2, pp. 168–186, 2012.
[37] Z. Hu and M.-H. Yang, "Learning good regions to deblur images," *Int. J. Comput. Vis.*, vol. 115, no. 3, pp. 345–362, 2015.
[38] Y.-W. Tai, P. Tan, and M. S. Brown, "Richardson-lucy deblurring for scenes under a projective motion path," *IEEE Trans. Pattern Anal. Mach. Intell.*, vol. 33, no. 8, pp. 1603–1618, Aug. 2011.
[39] Z. Hu and M.-H. Yang, "Fast non-uniform deblurring using constrained camera pose subspace," in *Proc. Brit. Mach. Vis. Conf.*, 2012, pp. 1–11.
[40] R. Köhler, M. Hirsch, B. Mohler, B. Schölkopf, and S. Harmeling, "Recording and playback of camera shake: Benchmarking blind deconvolution with a real-world database," in *Proc. Eur. Conf. Comput. Vis.*, 2012, pp. 27–40.
[41] S. Harmeling, H. Michael, and B. Schölkopf, "Space-variant single-image blind deconvolution for removing camera shake," in *Proc. Adv. Neural Inf. Process. Syst.*, 2010, pp. 829–837.
[42] H. Ji and K. Wang, "A two-stage approach to blind spatially-varying motion deblurring," in *Proc. IEEE Conf. Comput. Vis. Pattern Recognit.*, Jun. 2012, pp. 73–80.
[43] M. Hirsch, C. J. Schuler, S. Harmeling, and B. Schölkopf, "Fast removal of non-uniform camera shake," in *Proc. IEEE Int. Conf. Comput. Vis.*, Nov. 2011, pp. 463–470.
[44] L. Zhong, S. Cho, D. Metaxas, S. Paris, and J. Wang, "Handling noise in single image deblurring using directional filters," in *Proc. IEEE Conf. Comput. Vis. Pattern Recognit.*, Jun. 2013, pp. 612–619.
[45] D. Krishnan and R. Fergus, "Fast image deconvolution using hyper-Laplacian priors," in *Proc. Adv. Neural Inf. Process. Syst.*, 2009, pp. 1033–1041.
[46] Y. Zhou and N. Komodakis, "A MAP-estimation framework for blind deblurring using high-level edge priors," in *Proc. 13th Eur. Conf. Comput. Vis.*, 2014, pp. 142–157.
[47] K. Zhang, X. Gao, D. Tao, and X. Li, "Multi-scale dictionary for single image super-resolution," in *Proc. IEEE Conf. Comput. Vis. Pattern Recognit.*, Jun. 2012, pp. 1114–1121.
[48] Y.-W. Tai and S. Lin, "Motion-aware noise filtering for deblurring of noisy and blurry images," in *Proc. IEEE Conf. Comput. Vis. Pattern Recognit.*, Jun. 2012, pp. 17–24.
[49] L. Xu, C. Lu, Y. Xu, and J. Jia, "Image smoothing via L_0 gradient minimization," *ACM Trans. Graph.*, vol. 30, no. 6, 2011, Art. no. 174.
[50] Q. Xie *et al.* (2014). "On the optimal solution of weighted nuclear norm minimization." [Online]. Available: https://arxiv.org/abs/1405.6012
[51] W. Dong, L. Zhang, and G. Shi, "Centralized sparse representation for image restoration," in *Proc. IEEE Int. Conf. Comput. Vis.*, Nov. 2011, pp. 1259–1266.

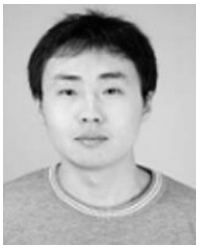

Wenqi Ren received the B.E. degree from the School of Information Engineering, Hebei University of Technology, in 2010, and the M.E. degree from the School of Computer Science and Communication Engineering, Tianjin University of Technology, in 2013. He is currently a joint-training Ph.D. student with the School of Computer Science and Technology at Tianjin University, China. He is currently pursuing the Ph.D. degree in electrical engineering and computer science with the University of California, Merced, CA, USA. His research interest includes image deblurring, image/video analysis and enhancement, and related vision problems.

Xiaochun Cao (SM'14) received the B.E. and M.E. degrees in computer science from Beihang University, Beijing, China, and the Ph.D. degree in computer science from the University of Central Florida, Orlando, FL, USA. After graduation, he spent about three years with the ObjectVideo Inc., as a Research Scientist. From 2008 to 2012, he was a Professor with Tianjin University, Tianjin, China. He has been a Professor with the Institute of Information Engineering, Chinese Academy of Sciences, China, since 2012. He has authored or co-authored over 120 journal and conference papers. He is a fellow of the IET. He serves on the Editorial Board of the IEEE TRANSACTIONS OF IMAGE PROCESSING. His dissertation was nominated for the University of Central Floridas University-Level Outstanding Dissertation Award. In 2004 and 2010, he was a recipient of the Piero Zamperoni Best Student Paper Award at the International Conference on Pattern Recognition.

Jinshan Pan is currently a joint-training Ph.D. student with the School of Mathematical Sciences, Dalian University of Technology, China. He is currently pursuing the Ph.D. degree in electrical engineering and computer science with the University of California at Merced, CA, USA. His research interest includes image deblurring, image/video analysis and enhancement, and related vision problems.

Xiaojie Guo (M'13) received the B.E. degree in software engineering from the School of Computer Science and Technology, Wuhan University of Technology, Wuhan, China, in 2008, and the M.S. and Ph.D. degrees in computer science from the School of Computer Science and Technology, Tianjin University, Tianjin, China, in 2010 and 2013, respectively. He is currently an Associate Professor with the Institute of Information Engineering, Chinese Academy of Sciences. He was a recipient of the Piero Zamperoni Best Student Paper Award in the International Conference on Pattern Recognition (International Association on Pattern Recognition), in 2010.

Wangmeng Zuo (M'09–SM'14) received the Ph.D. degree in computer application technology from the Harbin Institute of Technology, Harbin, China, in 2007. He was a Research Assistant with the Department of Computing, The Hong Kong Polytechnic University, Hong Kong, from 2004 to 2008. From 2009 to 2010, he was a Visiting Professor with Microsoft Research Asia, Beijing, China. He is currently an Associate Professor with the School of Computer Science and Technology, Harbin Institute of Technology. He has authored over 50 papers in the research areas. His current research interests include image modeling and low-level vision, discriminative learning, and biometrics. He is an Associate Editor of the IET Biometrics.

Ming-Hsuan Yang (M'92–SM'06) received the Ph.D. degree in computer science from the University of Illinois at Urbana–Champaign, USA, in 2000. He is currently an Associate Professor of Electrical Engineering and Computer Science with the University of California at Merced, CA, USA. He served as an Associate Editor of the IEEE TRANSACTIONS ON PATTERN ANALYSIS AND MACHINE INTELLIGENCE from 2007 to 2011, and he is an Associate Editor of the International *Journal of Computer Vision, Image and Vision Computing*, and *Journal of Artificial Intelligence Research*. He is a senior member of ACM. He received the NSF CAREER Award in 2012, and the Google Faculty Award in 2009.